第 32卷 第 1期 焊 接 学 报 Vol.32 No.1
2011年 1月 TRANSACTIONS OF THE CHINA WELDING INSTITUTION January 2011

双面双弧焊机器人主从协调运动控制

张华军[1,3]， 张广军[2]， 蔡春波[1]， 肖 俊[2]， 高洪明[2]

（1. 哈尔滨理工大学 材料科学与工程学院，哈尔滨 150040；
2. 哈尔滨工业大学 现代焊接生产技术国家重点实验室，哈尔滨 150001；
3. 上海交通大学 材料科学与工程学院，上海 200240）

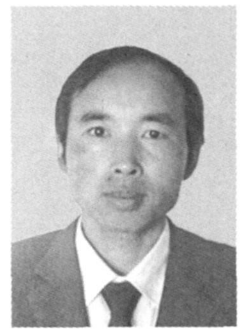

张华军

摘 要：为了实现低合金高强钢厚板机器人焊接，研究了一种不清根的双面双弧焊机器人柔性加工系统。系统采用集散控制，双面双机器人采用主从协调控制策略，Motoman机器人为主手（正面），KUKA机器人为从手（背面），建立该系统协调运动的算法模型，根据主手焊枪末端位置和姿态，以工件基准路径平面为对称面，经过运动学坐标变换，推导出背面从手机器人工具末端的运动路径点，从而控制从手跟随主手协调运动。经过双机器人协调试验，结果表明，该算法能满足双面双机器人焊接要求.

关键词：双面双弧焊；双机器人；主从控制；协调运动

中图分类号：TP242 文献标识码：A 文章编号：0253－360X（2011）01－0025－04

0 序 言

一种高效焊接方法双面双弧焊可不用清根[1]，大大简化了工艺，并且提高焊接生产率、减小变形和改善焊缝质量[2]，适合机器人焊接. 与单面单弧焊机器人相比，双面双弧焊机器人大大提高单位时间熔敷率、减小焊接变形、减少焊接缺陷、增大操作空间、减少示教任务等优点. 目前，双机器人空间复杂边缘有接触或无接触的跟踪[3]，主手把持工件，从手进行装配或焊接的双机器人协调运动模式的研究比较多[4,5]，通过确定双机器人协调运动的约束关系，然后将这一系列的约束关系作用到机器人末端操作器上，从而获得机器人协调运动的位置和姿态[6]. 文中提出的一种主从协调控制主要针对工件固定，工件两侧两机器人都进行焊接的模式，即从机器人根据主机器人末端位姿进行跟随协调运动，针对这种双面双机器人焊接协调控制还未见报道. 双面双机器人采用主从协调控制策略，根据主手焊枪末端位置和姿态，以工件基准路径平面为对称面，经过运动学坐标变换，推导出背面从手机器人工具末端的运动路径点，从而控制从手跟随主手协调运动，实现了双面双弧焊机器人焊接.

收稿日期：2010－11－29
基金项目：国家博士后科学基金资助项目（20090460616）；黑龙江省教育厅科技资助项目（20100503066）；哈尔滨市科技创新人才基金资助项目（2010RFQXG005）

1 双面双机器人集散控制系统

双面双弧焊工艺是针对厚板焊接效率以及自动化程度低下而提出的，其工作原理是打底焊时采用双面双脉冲 GTAW焊接，外送丝焊，两焊枪保持一定的间距，而填充和盖面焊采用双面双 GMAW焊，两焊枪保持对称，实现了双面双电弧焊接[1]. 目前，机器人控制系统的结构主要有三类，集中控制、分散控制和集散控制. 其中集散控制具有集中控制和分散控制的优点，既有一定的灵活性，又具有较高的协调能力[6]，文中系统采用集散控制，如图 1所示，通过离线编程仿真系统规划出主机器人的执行任务程序，下载到集中协调控制中心和主机器人控制器中，集中控制中心可以实现与双机器人的网络通讯，管理规划子任务，并执行调配任务，控制中心通过实时采集主机器人末端位姿的 6个参数，经过协调控制策略，可以推导出从机器人末端位姿的 6个参数，从而控制从机器人执行对称焊接任务.

主机器人采用 MOTOMAN机器人 UP20，从机器人采用 KUKA机器人 CR16. 打底焊，采用双面双 TIG焊，保持一定弧间距，主机器人执行打底焊子任务，同时后台计算出从机器人末端位姿参数并存储，经过时间 后，从机器人启动，调用已存储数据，延时执行背面打底焊，使双机器人保持一定的弧间距进行焊接；填充焊采用 MIG焊，换枪结束后，主机器人调用填充焊子任务，并执行任务，从机器人立刻采

集主机器人工具末端位姿, 经过双机器人协调算法可获得从机器人末端位姿参数, 而跟随执行背面填充任务, 此时双机器人同步, 即弧间距为零, 这时不需要存储数据, 实时获得从机器人末端位姿参数, 使从机器人跟随主机器人执行任务.

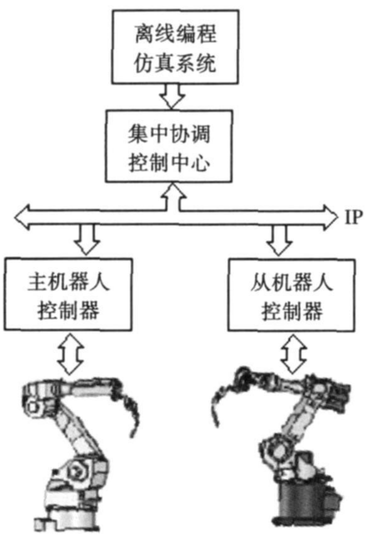

图 1 双机器人集散控制系统

Fig. 1 Distributed control system of double robots

2 双弧焊机器人主从协调控制模型

2.1 双机器人协调运动问题描述

图 2为双机器人协调运动变换矩阵示意图, 双机器人和试件的放置空间位姿是固定已知的, 并且主机器人焊枪末端相对于机器人基坐标系的位姿也是已知的, 可以通过集中控制中心获取到, 由式(1)可获得主机器人焊枪末端相对于工件坐标系的位姿矩阵, 通过与工件对称面进行对称矩阵转换, 可以求得从机器人焊枪末端相对于工件坐标系的位姿矩阵, 那么由式(2)可以计算出从机器人焊枪末端相对于机器人基坐标系的位姿矩阵, 即

$$ {}^{p}_{mt}T = {}^{w}_{p}T^{-1} \cdot {}^{w}_{mr}T \cdot {}^{mr}_{mt}T \tag{1} $$

$$ {}^{sr}_{st}T = {}^{w}_{sr}T^{-1} \cdot {}^{w}_{p}T \cdot {}^{p}_{st}T \tag{2} $$

式中: ${}^{w}_{mr}T$和${}^{w}_{sr}T$分别为主从机器人基坐标相对世界坐标系的姿态齐次变换矩阵; ${}^{mr}_{mt}T$和${}^{sr}_{st}T$分别为主从机器人工具坐标系相对主从机器人基坐标系的姿态齐次变换矩阵; ${}^{p}_{mt}T$和${}^{p}_{st}T$分别为主从机器人工具坐标系相对工件坐标系的姿态齐次变换矩阵; ${}^{w}_{p}T$为工件坐标系相对世界坐标系的位姿变换矩阵.

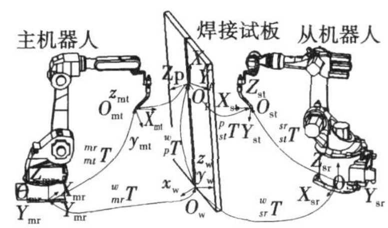

图 2 双机器人协调运动矩阵变换图

Fig. 2 Matrix transformation of double-robots coordinated motion

2.2 主从协调运动数学模型

集中协调控制系统获取主机器人的末端位姿参数为${}^{mr}_{mt}P_x$, ${}^{mr}_{mt}P_y$, ${}^{mr}_{mt}P_z$, α, β, γ, 根据该 6个参数可推导出${}^{mr}_{mt}T$. 焊枪末端姿态绕机器人基坐标{mr}旋转, 可采用 RPY方法, 即绕固定轴 X-Y-Z旋转. 设焊枪的初始方位{mt}与机器人基坐标系{mr}相重合, 首先将{mt}绕 X_{mr}轴旋转 γ角, 再绕 Y_{mr}轴旋转 β角, 绕 Z_{mr}轴旋转 α角, 按照"从右向左"原则得到相应的旋转矩阵.

$$ {}^{mr}_{mt}R_{xyz}(\gamma,\beta,\alpha) = R(Z_{mr},\alpha)\cdot R(Y_{mr},\beta)\cdot R(X_{mr},\gamma) = \begin{bmatrix} \cos\alpha & -\sin\alpha & 0 \\ \sin\alpha & \cos\alpha & 0 \\ 0 & 0 & 1 \end{bmatrix} \begin{bmatrix} \cos\beta & 0 & \sin\beta \\ 0 & 1 & 0 \\ -\sin\beta & 0 & \cos\beta \end{bmatrix} \begin{bmatrix} 1 & 0 & 0 \\ 0 & \cos\gamma & -\sin\gamma \\ 0 & \sin\gamma & 0 \end{bmatrix} \tag{3} $$

$$ {}^{mr}_{mt}T = \begin{bmatrix} \cos\alpha\cos\beta & \cos\alpha\sin\beta\sin\gamma - \sin\alpha\cos\gamma & \cos\alpha\sin\beta\sin\gamma + \sin\alpha\cos\gamma & {}^{mr}_{mt}P_x \\ \sin\alpha\cos\beta & \sin\alpha\sin\beta\sin\gamma + \cos\alpha\cos\gamma & \sin\alpha\sin\beta\sin\gamma - \cos\alpha\cos\gamma & {}^{mr}_{mt}P_y \\ -\sin\beta & \cos\beta\sin\gamma & \cos\beta\cos\gamma & {}^{mr}_{mt}P_z \\ 0 & 0 & 0 & 1 \end{bmatrix} \tag{4} $$

以工件平台原点为参考坐标系(世界坐标系){w}, 以工件轴对称中心线为基准路径, 沿焊缝方向为 X向, 焊板宽度方向为 Y向, 工件坐标系{p}, 即 XOY面为对称面, 考虑到该工艺是采用立焊, 可认为工件坐标 X_p与世界坐标 Z_w平行, 通过它们相互定位关系, 可确定工件相对于世界坐标系的位姿矩阵. 先绕 Z轴旋转 135°, 再绕 Y轴旋转 90°. 即可获得工件相对于世界坐标系旋转矩阵, 即

$$ {}^{w}_{p}R_{xyz}(135^\circ, 90^\circ, 0) = \begin{bmatrix} 0 & 0.707 & 0.707 \\ 0 & -0.707 & 0.707 \\ -1 & 0 & 0 \end{bmatrix} \tag{5} $$

$$ {}^{w}_{p}T^{-1} = \begin{bmatrix} 0 & -0.707 & -0.707 & -{}^{w}_{p}P_x \\ 0 & -0.707 & -0.707 & -{}^{w}_{p}P_y \\ 1 & 0 & 0 & 0 \\ 0 & 0 & 0 & 1 \end{bmatrix} \tag{6} $$

式中: ${}^{w}P_{px}$ 和 ${}^{w}P_{py}$ 为工件原点在平台原点的 x, y向距离, 可以通过测量获得.

工作平台与两机器人之间的位置和坐标系是固定的, 并且三个坐标系的 X向是平行的, 同样可确定出主从机器人相对于世界坐标系的齐次变换矩阵为

$$ {}^{w}_{mr}T = \begin{bmatrix} -1 & 0 & 0 & 0 \\ 0 & -1 & 0 & {}^{w}_{mr}P_y \\ 0 & 0 & 1 & {}^{w}_{mr}P_z \\ 0 & 0 & 0 & 1 \end{bmatrix} \tag{7} $$

$$ {}^{w}_{sr}T^{-1} = \begin{bmatrix} 1 & 0 & 0 & 0 \\ 0 & 1 & 0 & -{}^{w}_{sr}P_y \\ 0 & 0 & 1 & -{}^{w}_{mr}P_z \\ 0 & 0 & 0 & 1 \end{bmatrix} \tag{8} $$

则有

$$ {}^{p}_{mt}T = {}^{w}_{p}T^{-1} \circ {}^{w}_{mr}T \circ {}^{mr}_{mt}T = \begin{bmatrix} 0.707(\sin\alpha\cos\beta + \sin\beta) & 0.707(\sin\alpha\sin\beta\sin\gamma + \cos\alpha\cos\gamma - \cos\beta) & 0.707(\sin\alpha\sin\beta\sin\gamma - \cos\alpha\cos\gamma - \cos\beta\cos\gamma) & 0.707({}^{mr}_{mt}P_y - {}^{mr}_{mt}P_z - {}^{w}_{mr}P_y - {}^{w}_{mr}P_z) - {}^{w}_{p}P_x \\ 0.707(\sin\alpha\cos\beta + \sin\beta) & 0.707(\sin\alpha\sin\beta\sin\gamma + \cos\alpha\cos\gamma - \cos\beta) & 0.707(\sin\alpha\sin\beta\sin\gamma - \cos\alpha\cos\gamma - \cos\beta\cos\gamma) & 0.707({}^{mr}_{mt}P_y - {}^{mr}_{mt}P_z - {}^{w}_{mr}P_y - {}^{w}_{mr}P_z) - {}^{w}_{p}P_y \\ -\cos\alpha\cos\beta & -\cos\alpha\sin\beta\sin\gamma + \sin\alpha\cos\gamma & -\cos\alpha\sin\beta\sin\gamma - \sin\alpha\cos\gamma & -{}^{mr}_{mt}P_x \\ 0 & 0 & 0 & 1 \end{bmatrix} \tag{9} $$

可设

$$ {}^{p}_{mt}T = \begin{bmatrix} {}^{p}_{mt}n_x & {}^{p}_{mt}o_x & {}^{p}_{mt}a_x & {}^{p}_{mt}p_x \\ {}^{p}_{mt}n_y & {}^{p}_{mt}o_y & {}^{p}_{mt}a_y & {}^{p}_{mt}p_y \\ {}^{p}_{mt}n_z & {}^{p}_{mt}o_z & {}^{p}_{mt}a_z & {}^{p}_{mt}p_z \\ 0 & 0 & 0 & 1 \end{bmatrix} \tag{10} $$

以基准焊缝工件坐标系中的 $x_pO_py_p$ 面为对称面, 可获得从机器人末端在工件坐标系中的位姿为

$$ {}^{p}_{st}T = \begin{bmatrix} {}^{p}_{mt}n_x & {}^{p}_{mt}o_x & {}^{p}_{mt}a_x & {}^{p}_{mt}p_x \\ {}^{p}_{mt}n_y & {}^{p}_{mt}o_y & {}^{p}_{mt}a_y & {}^{p}_{mt}p_y \\ -{}^{p}_{mt}n_z & -{}^{p}_{mt}o_z & -{}^{p}_{mt}a_z & {}^{p}_{mt}p_y \\ 0 & 0 & 0 & 1 \end{bmatrix} \tag{11} $$

$$ {}^{sr}_{st}T = {}^{w}_{sr}T^{-1} \circ {}^{w}_{p}T \circ {}^{p}_{st}T \tag{12} $$

$$ {}^{sr}_{st}T = \begin{bmatrix} {}^{sr}_{st}n_x & {}^{sr}_{st}o_x & {}^{sr}_{st}a_x & {}^{sr}_{st}p_x \\ {}^{sr}_{st}n_y & {}^{sr}_{st}o_y & {}^{sr}_{st}a_y & {}^{sr}_{st}p_y \\ {}^{sr}_{st}n_z & {}^{sr}_{st}o_z & {}^{sr}_{st}a_z & {}^{sr}_{st}p_z \\ 0 & 0 & 0 & 1 \end{bmatrix} \tag{13} $$

最终需求出从机器人的末端位姿参数为 ${}^{sr}_{st}p_x$, ${}^{sr}_{st}p_y$, ${}^{sr}_{st}p_z$, α', β', γ', 因为集中控制系统是通过该 6个参数去控制从机器人的协调运动的.

假设已获得 ${}^{sr}_{st}p_x$, ${}^{sr}_{st}p_y$, ${}^{sr}_{st}p_z$, α', β', γ' 这 6个参数, 则同样可以采用 RPY的方法, 获得从机器人焊枪末端相对于基坐标{sr}姿态.

$$ {}^{sr}_{st}T = \begin{bmatrix} \cos\alpha'\cos\beta' & \cos\alpha'\sin\beta'\sin\gamma' - \sin\alpha'\cos\gamma' & \cos\alpha'\sin\beta'\sin\gamma' + \sin\alpha'\cos\gamma' & {}^{sr}_{st}p_x \\ \sin\alpha'\cos\beta' & \sin\alpha'\sin\beta'\sin\gamma' + \cos\alpha'\cos\gamma' & \sin\alpha'\sin\beta'\sin\gamma' - \cos\alpha'\cos\gamma' & {}^{sr}_{st}p_y \\ -\sin\beta' & \cos\beta'\sin\gamma' & \cos\beta'\cos\gamma' & {}^{sr}_{st}p_z \\ 0 & 0 & 0 & 1 \end{bmatrix} \tag{14} $$

联合上式, 需要求逆解, 即求出 α', β', γ'. 超越方程, 有 3个未知数 α', β', γ', 共有 9个方程, 其中 6个方程不独立, 因此可以利用其中 3个方程解出 3个未知数.

如果 $\beta' = 90^\circ$, 即 $\alpha' = 0$, $\gamma' = A\tan 2({}^{sr}_{st}o_x, {}^{sr}_{st}o_y)$; $\beta' = -90^\circ$, 即 $\alpha' = 0$, $\gamma' = -A\tan 2({}^{sr}_{st}o_x, {}^{sr}_{st}o_y)$.

如果 $\cos\beta' \neq 0$, 则各角的反正切表达式, 为

$$ \begin{cases} \alpha' = A\tan 2({}^{sr}_{st}n_y, {}^{sr}_{st}n_x) \\ \beta' = A\tan 2\left(-{}^{sr}_{st}n_z, \sqrt{({}^{sr}_{st}n_x)^2 + ({}^{sr}_{st}n_y)^2}\right) \\ \gamma' = A\tan 2({}^{sr}_{st}o_z, {}^{sr}_{st}a_z) \end{cases} $$

即可求出控制从机器人末端相对于机器人基坐标系的位姿的 6个控制参数.

3 协调算法验证试验及结果

采用示教盒手动操纵 Kuka机器人运动, 观察 Motoman机器人运动效果, 图 3为主从机器人在 xOy面的位移曲线图, 可看出从机器人基本复现了主机器人的轨迹, 但有一定的延迟, 这是由于通讯延迟和机器人种类差异的影响而造成的, 但其轨迹误差几乎为零. 但针对焊接来说, 一般焊接速度很小, 文中工艺采用的立向上焊, 其焊接速度为 1.2 mm/s, 速度很小, 尤其在主机器人采用梯形摆动焊接方式, 中间本身就有短暂的停顿, 研究发现这时从机器人的滞后性和停顿现象几乎消失, 可见, 能满足实际机器人摆动立向上焊接的工作要求.

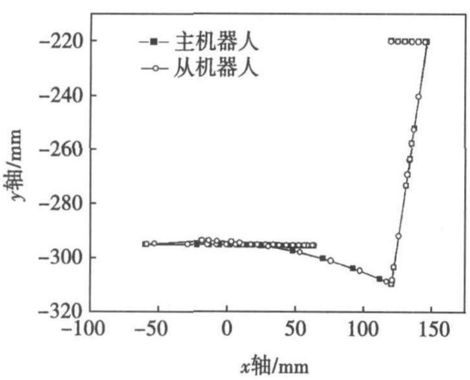

图 3 双机器人协调运动结果

Fig. 3 Coordinated motion results of double-sided robots

系统采用集散控制, 双面双机器人采用主从协调控制策略, Motoman机器人为主手 (正面), KUKA机器人为从手 (背面), 建立该系统协调运动的算法模型, 根据主手焊枪末端位置和姿态, 以工件基准路径平面为对称面, 经过运动学坐标变换, 推导出背面从手机器人工具末端的运动路径点, 从而控制从手跟随主手协调运动, 实现了双面双弧焊机器人焊接.

4 结 论

(1) 基于集散控制系统, 建立了双面双弧焊机器人主从协调运动数学模型, 以工件基准路径平面为对称面, 推导出从机器人工具末端的运动路径点.

(2) 双机器人主从协调运动试验结果表明, 从机器人完全复现主机器人的轨迹, 满足双面双弧摆动立焊生产要求.

参考文献:

[1] 张华军, 张广军, 王俊恒, 等. 低合金高强钢双面双弧焊热循环对组织性能影响[J]. 焊接学报, 2007, 28(10): 81-84.
Zhang Huajun, Zhang Guangjun, Wang Junheng, et al. Effect of thermal cycles of DSAW on microstructure in low alloy high strength steel[J]. Transactions of the China Welding Institution, 2007, 28(10): 81-84

[2] Zhang Huajun, Zhang Guangjun, Wu Lin. Effects of arc distance on angular distortion by asymmetrical double sided arc welding [J]. Science and Technology of Welding & Joining, 2007, 12(6): 564-571.

[3] 陈国良, 黄心汉, 王 敏. 双机器人协调完成复杂边缘跟踪的运动规划[J]. 电气自动化, 2006, 28(5): 253-257.
Chen Guoliang, Huang Xinhan, Wang Min. Motion planning for two cooperative robots tracking complex edge[J]. Electrical Automation, 2006, 28(5): 26-30.

[4] 王越超, 谈大龙. 协作机器人学的研究现状与发展[J]. 机器人, 1998, 20(1): 69-73.
Wang Yuechao, Tan Dalong. Cooperative robotics research and development status[J]. Robot, 1998, 20(1): 69-73.

[5] 朴永杰. 焊接柔性制造单元多智能体协调控制的研究[D]. 上海: 上海交通大学, 2004.

[6] 曲道奎, 谈大龙, 张春杰, 等. 双机器人协调控制系统[J]. 机器人, 1991, 13(3): 6-11.
Qu Daokui, Tan Dalong, Zhang Chunjie, et al. Two cooperative robotics control system[J]. Robot, 1991, 13(3): 6-11.

作者简介: 张华军, 男, 1978年出生, 博士, 副教授. 主要从事高效焊接及机器人焊接自动化方向. 发表论文 30余篇. Email: huajunzhang@126.com anyong[2], WANG Qing, DAI Zhen[3] (1. School of Material Science and Engineering, Tianjin University, Tianjin 300072, China; 2. Tianjin Key Laboratory of Advanced Joining Technology, Tianjin 300072, China; 3. Hebei Electric Power Research Institute, Shijiazhuang 050021, China). p 16—20

Abstract: Type IV cracking is considered to be the likely failure mode of P92 steel welds when operated at high temperature for long duration. Type IV failure often takes place at the intercritical heat affected zone (ICHAZ) or fine grained heat affected zone (FGHAZ). However, the mechanism of type IV cracking has not yet been understood unequivocally. In order to investigate type IV failure scientifically, temperature field, welding residual stress and creep strain for welded joint of P92 steel are simulated by ABAQUS code. Experimental result obtained from X-ray diffraction technique is conducted to verify the simulation. The research results show that the locations of ICHAZ and FGHAZ are demonstrated according to the simulation of temperature field. Maximal residual stress concentrates in the ICHAZ and FGHAZ. And axial creep strain is in good agreement with residual stress. So concentration of residual stress that results in accumulation of creep strain and type IV cracking is regarded as remarkable factor.

Key words: P92 steel; type IV cracking; temperature field; welding residual stress; finite element simulation

Relations between 3-dimension interface topography with thermal stress of thermal barrier coatings WANG Zhiping, HAN Zhiyong, CHEN Yajun, DING Kunying (Institute of Material Technology, Civil Aviation University of China, Tianjin 300300, China). p 21—24

Abstract: Double layer thermal barrier coatings (bond coating is NiCrAlY and ceramic coating is ZrO_2) was prepared by atmospheric plasma sprayed method. Using ABAQUS software, the thermal stress distribution of 3-dimension ellipse interface topography between bond coating and ceramic coating was numerically simulated by indirect coupling method. Relations between thermal stress with location and size of ellipse topography unit were obtained. The calculating results show that the stress is affected by location and size obviously and stress of boundary topography unit is bigger than that of center unit when the size of unit is invariable. The boundary topography units are danger unit and corner points are danger points. The stress of danger point reaches 324 MPa when short half axes is 20.

Key words: thermal barrier coatings; thermal stress; interface topography

Master-slave coordinated motion controlling of double-sided arc welding robots ZHANG Huajun[1,3], ZHANG Guangjun[2], CAI Chunbo[2], XIAO Jun[2], GAO Hongming[2] (1. School of Materials Science and Engineering, Harbin University of Science and Technology, Harbin 150040, China; 2. State Key Laboratory of Advanced Welding Production Technology, Harbin Institute of Technology, Harbin 150001, China; 3. School of Material Science and Technology, Shanghai Jiaotong University, Shanghai 200240, China). p 25—28

Abstract: A flexible manufacturing system of non root chipping double-sided arc welding robots is studied in order to realize robot automatic welding for thick plate of low alloy high tensile steel. Master-slave coordinated method is adopted. Motoman robot is master and KUKA robot is slave. According to the ending position attitude of welding torch of master hand, reference path plane of plate is look on as symmetric plane. Motion path of slave-hand is deduced by kinematics coordinate conversion. And Master-slave coordinated motion of double-sided arc welding robots is reached and is verified by coordinated motion experiment.

Key words: double-sided arc welding; double robots; master-slave control; coordinated motion

Comprehensive evaluation on effect of weld shape on mechanical performances by analytic hierarchy process LIU Xin[1,2], LEI Yongping[1], GONG Shuili[2] (1. Beijing University of Technology, Beijing 100010, China; 2. Science and Technology on Power Beam Processes Laboratory, Beijing Aeronautical Manufacturing Technology Research Institute, Beijing 100024, China). p 29—32

Abstract: Four different weld shapes are obtained by proper electron beam welding parameters, which are respectively named as bell shape, funnel shape, nail shape and wedge shape. Mechanical performance of the electron beam welded joints with different shapes were carried. The influence of weld shape on mechanical performance of the joints was synthetically evaluated by analytic hierarchy mathematical model. The results show that weld shape effects tensile property, fatigue property and microhardness of the joint. The sequencing of mechanical performance of the joints with four different shapes by analytic hierarchy process is bell shape, funnel shape, wedge shape, and nail shape. It is validated by experimental results that the analytic hierarchy mathematical model is effective and practical.

Key words: weld shape; electron beam welding; mechanical performance; analytic hierarchy process

Effects of welding parameters on weld geometry of pulsed Nd:YAG laser/TIG hybrid welding process of 304 stainless steel ZHANG Linjie[1], ZHANG Jianxun[1], CAO Weijie[1], CHAI Guoming[1], GONG Shuili[2] (1. State Key Laboratory of Mechanical Behavior for Materials, Xi'an Jiaotong University, Xi'an 710049, China; 2. National key Laboratory for High Energy Density Beam Processing Technology, Beijing Aeronautical Manufacturing Technology Research Institute, Beijing 100024, China). p 33—36

Abstract: Effects of welding parameters on the weld geometry are investigated for pulsed Nd:YAG laser/TIG hybrid welding of 304 stainless steel plate. The results show that cross sectional area of hybrid weld is larger than the sum of cross sectional area of single laser weld and that of single TIG weld, which means synergetic effect occurs during hybrid welding process; weld width, weld depth, weld cross sectional area and heat transfer efficiency increase with the increase of laser power; when defocusing distance increase from -3mm to 5mm, weld width, weld depth, weld cross sectional area and heat transfer efficiency would increase and reach the maximum when defocus-